A Comprehensive Standardized Model for Ultrawideband Propagation Channels

Andreas F. Molisch, *Fellow, IEEE*, Dajana Cassioli, *Member, IEEE*, Chia-Chin Chong, *Member, IEEE*, Shahriar Emami, *Senior Member, IEEE*, Andrew Fort, *Member, IEEE*, Balakrishnan Kannan, *Member, IEEE*, Johan Karedal, *Student Member, IEEE*, Juergen Kunisch, Hans Gregory Schantz, *Senior Member, IEEE*, Kazimierz Siwiak, *Senior Member, IEEE*, and Moe Z. Win, *Fellow, IEEE*

***Abstract*—A comprehensive statistical model is described for ultrawideband (UWB) propagation channels that is valid for a frequency range from 3–10 GHz. It is based on measurements and simulations in the following environments: residential indoor, office indoor, builtup outdoor, industrial indoor, farm environments, and body area networks. The model is independent of the used antennas. It includes the frequency dependence of the path gain as well as several generalizations of the Saleh–Valenzuela model, like mixed Poisson times of arrival and delay-dependent cluster decay constants. A separate model is specified for the frequency range below 1 GHz. The model can thus be used for realistic performance assessment of UWB systems. It was accepted by the IEEE 802.15.4a Task Group as standard model for evaluation of UWB system proposals. This paper also presents a critical assessment of the applicability of the model and possible generalizations and improvements.**

***Index Terms*—Delay dispersion, statistical channel model, ultrawideband (UWB), wireless propagation.**

I. Introduction

ULTRAWIDEBAND (UWB) communications systems are commonly defined as systems that have either more than 20% relative bandwidth or more than 500 MHz absolute bandwidth. UWB communications originally started with the spark-gap transmitter of Hertz and Marconi. However, it was not until the 1990s that the interest was renewed. The pioneering work in [1]–[6] developed the concept of time-hopping impulse radio systems. In 2002, the frequency regulator in the United States allowed unlicensed UWB transmission (subject to the fulfillment of spectral masks), and other countries are expected to follow suit. This gave rise to a large volume of theoretical as well as practical work on system designs using UWB signaling (see, for example, [7]–[9] for a general overview, [10]–[13] for impulse radio, [14] for frequency-hopping orthogonal frequency-division multiplexing system, and [15] for direct-sequence spread spectrum (DS-SS) systems).

The large bandwidth of UWB systems leads to several important advantages, including:

- low interference to and from other systems;
- low sensitivity to fading [16]–[18];
- accurate position location and ranging due to the fine time resolution [19];
- possible easier material penetration.

One of the most promising applications for UWB are sensor networks, where a large number of sensor nodes communicate among each other, and with central nodes, with high reliability [20]. The data rates for those applications are typically low (<1 Mbit/s), and the good ranging and geolocation capabilities of UWB are particularly useful. Recognizing these developments, the IEEE has established the standardization group 802.15.4a, which is currently in the process of developing a standard for these applications.

The ultimate performance limits of a communications systems, as well as the performance of practical systems, are determined by the channel it operates in [21]. Realistic channel models are thus of utmost importance for system design and testing. However, UWB propagation channels show fundamental differences from conventional (narrow-band) propagation in many respects [22]–[24], so that the established (narrow-band) channel models [25] cannot be used; this has a significant impact on system design [26]–[28]. A number of UWB channel models have been proposed in the past: [29] suggested a model for the frequency range below 1 GHz. The IEEE 802.15.3a group developed a channel model [30] that is valid from 3 to 10 GHz but is designed only for indoor residential and office environments, and the distance between transmitter and receiver is restricted to <10 m. A considerable number of papers has been published on the measurement and modeling for specific environments (see [24] for an overview), but none of them has gained widespread acceptance for system testing purposes.

In this paper, we present a general model for UWB channels that is valid for the high-frequency range (3–10 GHz) in a number of different environments as well as for the frequency

Manuscript received 2005; revised March 2006. This paper was presented in part at IEEE GLOBECOM 2005, St. Louis, MO, No. 28–Dec. 2, 2005.

A. F. Molisch is with Mitsubishi Electric Research Labs, Cambridge, MA 02139 USA and also with the Department of Electroscience, Lund University, Lund, Sweden (e-mail: Andreas.Molisch@ieee.org).

D. Cassioli is with RadioLabs, University of L'Aquila, Poggio di Roio, L'Aquila, Italy (e-mail: cassioli@ing.univaq.it).

C.-C. Chong was with Samsung Advanced Institute of Technology, Suwon, South Korea. She is now with DoCoMo Communications Laboratories USA Inc., Palo Alto, CA 94304 USA (e-mail: Chia-Chin.Chong@ieee.org).

S. Emami is with Focus Enhancements Semiconductor, Hillsboro, OR 97124 USA (e-mail: Shahriare@focussemi.com).

A. Fort is with IMEC, Belgium (e-mail: forta@imec.be).

B. Kannan was with A* STAR, Singapore. He is now with the University of New South Wales, Sydney 2052, Australia (e-mail: bkannan@ee.usyd.edu.au).

J. Karedal is with the Department of Electroscience, Lund University, Lund, Sweden (e-mail: Johan.Karedal@es.lth.se).

J. Kunisch is with IMST GmbH, Kamp-Lintfort, Germany (e-mail: kunisch @imst.de).

H. G. Schantz is with Q-track Corporation, Huntsville, AL 35816 USA.

K. Siwiak is with TimeDerivative, Inc., Coral Springs, FL 33077 USA (e-mail: kai@timederivative.com).

M. Z. Win is with the Massachusetts Institute of Technology, Cambridge, MA 02139 USA (e-mail: moewin@mit.edu).

Digital Object Identifier 10.1109/TAP.2006.883983

range below 1 GHz in office environments; the model is based on measurements and simulations of the authors [31]–[36] and other papers in the open literature. The model has been developed by the authors during their work for the 802.15.4a group, and was accepted by that body as the official model for comparing different system proposals for standardization. The value of this paper is thus threefold.

- It represents a model for UWB channels that is accepted by an official standardization body for the purpose of selecting among physical layer proposals and is available for a large number of environments.
- It includes a number of refinements and improvements beyond what the authors and others had previously presented in the literature, specifically:
  - — frequency dependence of the path gain, and thus implicitly the distortions of each separate multipath component (MPC);
  - — modeling of the number of clusters of MPCs in the Saleh–Valenzuela (S–V) model as a random variable;
  - — a power delay profile that models a "soft" onset, so that the first arriving paths can be considerably weaker than later MPCs; this is critical for accurate assessment of ranging capabilities of UWB;
  - — a new model for body-area networks that includes correlated lognormal shadowing.
- It critically discusses the advantages and drawbacks of the model, especially limits of applicability. It also describes possible future improvements, and in particular suggests a generalization of the model for body-area networks based on measurements that were performed after the standard model was fixed.

It is a widespread misunderstanding that the 15.4a channel model is suitable only for low-data-rate UWB systems, because it was developed within the framework of the standardization of low-data-rate systems. We stress that the 15.4a channel model is valid for UWB systems *irrespective of their data rate and their modulation format*.

The remainder of this paper is organized as follows. In Section II, we present the generic channel model structure, especially discussing the refinements compared to previous literature. Section III describes the actual parameterization in different environments, while Section IV concentrates on the channel model for body-area networks, which has a slightly different underlying structure. Next, we discuss how the model should be implemented and used for system testing. Section VI shows some example results for power delay profiles and other parameters characterizing the delay dispersion. A summary concludes this paper.

II. Generic Channel Model

A. Frequency Range

The Federal Communications Commission (FCC) ruling [37] specifies two admissible frequency ranges for intentional UWB emissions: 3.1–10.6 GHz and <1 GHz. In both of those ranges, there are restrictions with respect to the admissible applications. For the 3.1–10.6 GHz range, indoor communications (with the exception of toys) as well as outdoor peer-to-peer communications, medical imaging, and surveillance are allowed. For the <1 GHz range, ground-penetrating radar applications are allowed; furthermore, a number of military applications operate in that frequency range.[1] Given the large range of admissible (and practically relevant) applications, the baseline draft of the IEEE 802.15.4a standard [39] foresees systems in both the 3.1–10.6 GHz range (or a subset thereof) and in the <1 GHz range. Consequently, channel models are required for both these frequency ranges.

B. Environments

The following environments have a high importance for sensor network applications and are those ones for which the model is parameterized

1) *Indoor residential:* These environments are critical for "home networking," linking different appliances, as well as safety (fire, smoke) sensors over a relatively small area. The building structures of residential environments are characterized by small units, with indoor walls of reasonable thickness.
2) *Indoor office:* Some of the rooms are comparable in size to residential, but other rooms (especially cubicle areas, laboratories, etc.) are considerably larger. Areas with many small offices are typically linked by long corridors. Each of the offices typically contains furniture, bookshelves on the walls, etc., which adds to the attenuation given by the (often thin) office partitionings.
3) *Outdoor:* While a large number of different outdoor scenarios exist, the current model covers only a suburban-like microcell scenario, with a rather small range.
4) *Industrial environments:* Characterized by larger enclosures (factory halls), filled with a large number of metallic reflectors. This is anticipated to lead to severe multipath.
5) *Agricultural areas/farms:* For those areas, few propagation obstacles (silos, animal pens), with large distances in between, are present. The delay spread can thus be anticipated to be smaller than in other environments.
6) *Body-area network (BAN):* Communication between devices located on the body, e.g., for medical sensor communications, "wearable" cellphones, etc. Note that this environment is related to fundamentally different propagation effects, and thus also uses a different generic channel model (see Section IV).

This list is not complete, and other environments can be important for specific applications (for example, propagation through snow for the detection of, and communication with, avalanche victims [40]). However, at the time of the drafting of the model, no measurements were available for those other environments. One viable way of extending the model in the future is to parameterize the generic model presented here for alternative environments, based on future measurement campaigns.

[1] A recently proposed ruling in Japan foresees that emissions within 3.4 and 4.8 GHz are admissible when a detect-and-avoid mechanism is used, while emissions at frequency ranges above 7.25 GHz would be admissible without such a mechanism [38]. Preliminary investigations of the European frequency regulators point towards similar rulings.

C. Path Gain

A key parameter for any wireless system is the path gain, i.e., the ratio of the received power (averaged over both the small-scale and the large-scale fading) to the transmit power.[2] The path gain determines the average signal-to-noise ratio (SNR) that a system can achieve. For UWB systems, the path gain at different frequencies can be noticeably different. This is related to the fact that the free-space attenuation, as well as the effect of basic propagation processes like diffraction and reflection at dielectric walls, changes with frequency. Specifically, we introduce a *frequency-dependent path gain*, which we define as

$$G(f,d) = \frac{1}{\Delta f} E\left\{ \int_{f-\Delta f/2}^{f+\Delta f/2} \left| H(\widetilde{f},d) \right|^2 d\widetilde{f} \right\} \tag{1}$$

where $H(f,d)$ is the transfer function from transmitter (TX) to receiver (RX), including the antennas (i.e., measured between the TX antenna connector and the RX antenna connector). The expectation $E\{\cdot\}$ is taken over the small-scale and large-scale fading. The frequency range Δf is chosen small enough so that diffraction coefficients, dielectric constants, etc., can be considered constant within that bandwidth. This definition is similar in spirit to Bello's quasi-stationary assumption [41], where the fading statistics are defined over a temporal range over which no significant changes of the average path gain are to be anticipated.

To simplify computations, we assume that the path gain as a function of the distance and frequency can be written as a product of the terms

$$G(f,d) = G(f) \cdot G(d). \tag{2}$$

We stress that this is an assumption made for modeling convenience, and is not based on measurements. The frequency dependence of the channel path gain is modeled as [34], [42], [43]

$$\sqrt{G(f)} \propto f^{-\kappa} \tag{3}$$

where κ is the frequency dependency decaying factor. The total path gain shows a monotonic distance dependence (modeled by a conventional power law) as well as random variations due to shadowing (which are modeled as lognormally distributed)

$$G_{\mathrm{dB}}(d) = G_0 - 10n\log_{10}\left(\frac{d}{d_0}\right) \tag{4}$$

where the reference distance d_0 is set to 1 m, G_0 is the path gain at the reference distance. The path gain exponent n depends on whether or not a line-of-sight (LOS) connection exists between the TX and RX. Note that we do not use a breakpoint model, but rather a single-slope power decay law. Added (on a decibel scale) to the pathgain is the shadowing gain S, which is (again in decibels) a Gaussian-distributed random variable with zero mean and standard deviation σ_S.[3]

[2]Note that we define a path gain G and not a path loss. Therefore, the path gain is smaller than unity (on a linear scale), or negative on a decibel scale.

[3]For the simulations within the 802.15.4a standardization, the shadowing is *not* taken into account.

D. Incorporation of Antenna Effects

In the 15.4a model, (1)–(4) refer to the propagation channel only, excluding antenna effects. It is actually an important aspect that the model tries to be independent of the frequency characteristics of the used antennas. This is all the more important as the frequency response of UWB antennas can vary wildly, depending on the antenna type, matching network, etc. [44]. The model therefore gives the frequency dependence of the channel alone, and leaves it to the user to combine it with the frequency characteristics of the antennas.

The frequency-dependent path gain can be related to the frequency characteristics of the antennas and of the environment.

1) In a first step, define the transmit power spectrum that will be seen "on air." This spectrum is the product of the output spectrum of the transmit amplifier, i.e., as seen at the antenna connector (it will in many cases approximate the FCC mask quite well) with the frequency-dependent antenna efficiency $\eta_{\mathrm{TX-ant}}(f)$.[4]

$$P_t(f) = P_{\mathrm{TX-amp}}(f) \cdot \eta_{\mathrm{TX-ant}}(f). \tag{5}$$

Note that in this step, we neglect the directional characteristics of the antenna. If the directional and frequency characteristics of both channel and antennas are separable, then the above equation can be interpreted as being valid in any particular direction when multiplied with the antenna gains in those directions.

2) In a next step, compute the frequency-dependent power density at a distance d as

$$\widehat{P}(f,d) = K_0 \frac{P_t(f)}{4\pi d_0^2}\left(\frac{d}{d_0}\right)^{-n}\left(\frac{f}{f_c}\right)^{-2\kappa} \tag{6}$$

where the normalization constant K_0 will be determined below. Note that this reverts to the conventional picture of energy spreading out equally over the surface of a sphere when we set $n = 2$, and $\kappa = 0$.

3) Then, the received frequency-dependent power has to be determined by multiplying the power density at the location of the receiver i) with the antenna area $A_{\mathrm{RX}} = G_{\mathrm{RX}}(f)\lambda^2/(4\pi)$, where G_{RX} is the receive antenna gain, and ii) with the antenna efficiency $\eta_{\mathrm{RX-ant}}(f)$. If we are assuming that the radiation is averaged over all incident angles, the antenna gain (averaged over the different directions) is unity, independent of the considered frequency. The frequency-dependent received power is then given by

$$P_{\mathrm{r}}(d,f) = K_0 P_{\mathrm{TX-amp}}(f) \cdot \eta_{\mathrm{TX-ant}}(f) \cdot \eta_{\mathrm{RX-ant}}(f) \frac{c_0^2}{(4\pi d_0 f_c)^2} \cdot \frac{1}{(d/d_0)^n (f/f_c)^{2\kappa+2}} \tag{7}$$

where c_0 is the speed of light. The normalization constant K_0 has to be chosen in such a way that the attenuation at distance $d_0 = 1$ m (the reference distance for all of our scenarios) and at the reference frequency $f_c = 5$ GHz is equal to a value G_0 that will be given later in the tables,

[4]Note that the frequency dependence of the antenna gain does not play a role here, as it only determines the distribution of the energy over the spatial angles—but our computations average over the spatial angle.

under the assumption of an ideally efficient, isotropic antenna. Thus

$$\frac{P_{\mathrm{r}}(d_0, f_c)}{P_{\mathrm{TX-amp}}(f_c)} = G_0 = K_0 \frac{c_0^2}{(4\pi d_0 f_c)^2} \tag{8}$$

so that

$$K_0 = \frac{(4\pi d_0 f_c)^2}{c_0^2} G_0. \tag{9}$$

4) Finally, it has been shown that at frequencies removed from the whole-body resonance region (30–300 MHz), the presence of a person (user) close to the antenna will lead to an attenuation. Measurements have shown this process to be stochastic, with attenuations varying between 1 and more than 10 dB, depending on the user to antenna coupling variation [45]. However, the model describes this effect by an "antenna attenuation factor" A_{ant} of 1/2 that is deterministic and has to be included in all computations. We therefore find the frequency-dependent path gain to be given by

$$G(f) = \frac{P_{\mathrm{RX}}(f)}{P_{\mathrm{TX-amp}}(f)} = \frac{1}{2} \cdot G_0 \cdot \eta_{\mathrm{TX-ant}}(f) \cdot \eta_{\mathrm{RX-ant}}(f) \cdot \frac{(f/f_c)^{-2(\kappa+1)}}{(d/d_0)^n}. \tag{10}$$

We stress again that the above derivation neglects the interdependence between the direction of the radiation and the directivity of the antennas.

E. Power Delay Profile (PDP)

The impulse response (in complex baseband) of the SV model is given in general as [46]

$$h_{\mathrm{discr}}(t) = \sum_{l=0}^{L} \sum_{k=0}^{K} a_{k,l} \exp(j\phi_{k,l}) \delta(t - T_l - \tau_{k,l}) \tag{11}$$

where $a_{k,l}$ is the tap weight of the kth component in the lth cluster, T_l is the delay of the lth cluster, and $\tau_{k,l}$ is the delay of the kth MPC relative to the lth cluster arrival time T_l. The phases $\phi_{k,l}$ are uniformly distributed, i.e., for a bandpass system, the phase is taken as a uniformly distributed random variable from the range [0,2π]. Note that this model implies that the path gain is independent of frequency; we will show below how this can be generalized to include the effects described in Sections II-C and -D.

The standard SV model does not specify the number of occuring clusters. Rather, the number of clusters is (theoretically) infinite, but their strength decreases exponentially with time; for practical purposes, an (arbitrary) threshold needs to be introduced, so that clusters with a strength below that threshold are not further considered in the simulations. This is problematic for standardization purposes, as performance evaluations by different research groups cannot be compared in a fair way if those groups use different thresholds. We solved this problem by modeling the number of clusters as a random variable with (typically) small mean value. Specifically, following [47], the number of clusters L is modeled as Poisson-distributed with probability density function (pdf)

$$pdf_L(L) = \frac{(\overline{L})^L \exp(-\overline{L})}{L!} \tag{12}$$

so that the mean $\overline{L}$ completely characterizes the distribution.

By definition, we have $\tau_{0,l} = 0$. The distributions of the cluster arrival times are given by a Poisson process so that the inter-cluster arrival times are exponentially distributed

$$p(T_l | T_{l-1}) = \Lambda_l \exp\left[-\Lambda_l (T_l - T_{l-1})\right],\ l > 0 \tag{13}$$

where Λ_l is the cluster arrival rate (assumed to be independent of l). The classical SV model also uses a Poisson process for the ray arrival times. Due to the discrepancy in the fitting for the indoor residential, indoor office, and outdoor environments, we model ray arrival times with a mixture of two Poisson processes as follows [33]:

$$p(\tau_{k,l} | \tau_{(k-1),l}) = \beta \lambda_1 \exp\left[-\lambda_1 \left(\tau_{k,l} - \tau_{(k-1),l}\right)\right] + (1-\beta)\lambda_2 \exp\left[-\lambda_2 \left(\tau_{k,l} - \tau_{(k-1),l}\right)\right],\ k > 0 \tag{14}$$

where β is the mixture probability, while λ_1 and λ_2 are the ray arrival rates.

For some environments, most notably the industrial environment, a "dense" arrival of MPCs was observed, i.e., each resolvable delay bin contains significant energy. In that case, the concept of ray arrival rates loses its meaning, and a realization of the impulse response based on a tapped delay line model with regular tap spacings is to be used.

The next step is the determination of the cluster powers and cluster shapes. The PDP (mean power of the different paths) is exponential within each cluster

$$E\left\{|a_{k,l}|^2\right\} \propto \Omega_l \exp(-\tau_{k,l}/\gamma_l) \tag{15}$$

where Ω_l is the integrated energy of the lth cluster and γ_l is the intracluster decay time constant.

Another important deviation from the classical SV model is that we find the cluster decay time to depend on the arrival time of the cluster. In other words, the larger the delay, the larger the decay time of the cluster. A linear dependence

$$\gamma_l = k_\gamma T_l + \gamma_0 \tag{16}$$

where k_γ describes the increase of the decay constant with delay, gives good agreement with measurement values.

The energy of the lth cluster, normalized to γ_l and averaged over the cluster shadowing and the small-scale fading, follows in general an exponential decay

$$10\log(\Omega_l) \propto 10\log\left(\exp(-T_l/\Gamma)\right) + M_{\mathrm{cluster}} \tag{17}$$

where M_{cluster} is a normally distributed variable with standard deviation $\sigma_{\mathrm{cluster}}$.

For the non-LOS (NLOS) case of some environments (office and industrial), the above description is not a good model for the PDP. Rather, we observe only a single cluster, whose power first

increases (with increasing delay), goes through a maximum, and then decreases again. Such a shape of the PDP can significantly influence the ranging and geolocation performance of UWB systems, as ranging algorithms require the identification of the first (not the strongest) MPC.

We found in the course of our investigation that the following functional fit gives a good description:

$$E\left\{|a_{k,1}|^2\right\} \propto (1-\chi\cdot\exp(-\tau_{k,l}/\gamma_{\rm rise}))\cdot\exp(-\tau_{k,l}/\gamma_1). \tag{18}$$

Here, the parameter χ describes the attenuation of the first component, the parameter $\gamma_{\rm rise}$ determines how fast the PDP increases to its local maximum, and γ_1 determines the decay at later times.

F. Small-Scale Fading

For narrow-band systems, complex Gaussian fading is conventionally used to describe the small-scale fading. More precisely, the equivalent complex baseband representation consists of a Rayleigh-distributed amplitude and a uniformly distributed phase. This can be related theoretically to the fact that a large number of MPCs falls into each resolvable delay bin, so that the central limit theorem is valid [21], [48]. In UWB systems, this is not true anymore, and a number of alternative amplitude distributions have been proposed in the literature (for an overview, see [24]). Our model describes the distribution of the small-scale amplitudes $|a_{k,l}|$ as Nakagami

$$pdf(x) = \frac{2}{\Gamma(m)}\left(\frac{m}{\Omega}\right)^m x^{2m-1}\exp\left(-\frac{m}{\Omega}x^2\right) \tag{19}$$

where $m \geq 1/2$ is the Nakagami m-factor, $\Gamma(m)$ is the gamma function, and Ω is the mean-square value of the amplitude. A conversion to a Rice distribution is approximately possible if $m \geq 1$ [49]

$$K_{\rm r} = \frac{\sqrt{m^2-m}}{m-\sqrt{m^2-m}} \tag{20}$$

where $K_{\rm r}$ is the Rice factor.[5]

The m-parameter is modeled as a lognormally distributed random variable, whose logarithm has a mean μ_m and standard deviation σ_m. Both of these can have a delay dependence

$$\mu_m(\tau) = m_0 - k_m\tau \tag{21}$$

$$\sigma_m(\tau) = \widehat{m}_0 - \widehat{k}_m\tau. \tag{22}$$

For the first component of each cluster, the Nakagami factor is modeled differently. It is assumed to be deterministic and independent of delay

$$m = \widetilde{m}_0. \tag{23}$$

[5]Note that the above representation is different from both [30] and [29], which used a (real) baseband model.

TABLE I
PARAMETERS FOR CHANNEL MODELS CM 1 AND CM 2 (RESIDENTIAL)

Residential	LOS	NLOS
valid range of d	$7-20$ m	$7-20$ m
Path gain		
G_0 [dB]	-43.9	-48.7
n	1.79	4.58
$S[dB]$	2.22	3.51
κ	1.12	1.53
Power delay profile		
$\overline{L}$	3	3.5
Λ [1/ns]	0.047	0.12
λ_1, λ_2 [1/ns],β	$1.54, 0.15, 0.095$	$1.77, 0.15, 0.045$
Γ [ns]	22.61	26.27
k_γ	0	0
γ_0 [ns]	12.53	17.50
$\sigma_{\rm cluster}$ [dB]	2.75	2.93
Small-scale fading		
m_0 [dB]	0.67	0.69
$\widehat{m}_0$ [dB]	0.28	0.32
$\widetilde{m}_0$	NA	NA

III. MODEL PARAMETERIZATION

A. Parameterization for 3–10 GHz Range

The parameters of the model are extracted by fitting measurement data to the model described in Section II. Guidelines for the extraction of the parameters from measurement values were established in the final report [50] but were not used for the evaluation of all available measurements. It must be noted that especially the extraction of cluster parameters is subject to a certain arbitrariness: a reasonably continuous PDP can often be interpreted either as a single cluster or as the sum of many, closely spaced clusters. A least squares fit can be used, but is sensitive to small variations and even noise. For this reason, the determination of the number of clusters was often done by "visual inspection."

Another important aspect of the evaluation concerns the frequency range of the model. The measurements and simulations that form the basis of the model in the different environments cover different frequency ranges. For use within the IEEE standardization, they are defined to be used for the whole 3.1–10.6 GHz range.[6] However, from a scientific point of view, they should only be used in the frequency range for which the underlying measurements are valid; those frequency ranges are specified in Tables I–IV. A similar statement is true for the distance between TX and RX over which the model should be used.

[6]Actually, the models were even used for evaluations in the 2–3.1 GHz range, in order to allow a fair comparison between narrow-band systems operating in the 2.45 GHz ISM band and UWB systems in the 3.1–10.6 GHz range.

TABLE II
PARAMETERS FOR CHANNEL MODELS CM 3 AND CM 4 (OFFICE)

Office	LOS	NLOS
valid range of d	$3-28$ m	$3-28$ m
Path gain		
n	1.63	3.07
σ_S	1.9	3.9
G_0 [dB]	-35.4	-59.9
κ	0.03	0.71
Power delay profile		
$\overline{L}$	5.4	1
Λ [1/ns]	0.016	NA
λ_1, λ_2 [1/ns],β	0.19, 2.97, 0.0184	NA
Γ [ns]	14.6	NA
k_γ	0	NA
γ_0 [ns]	6.4	NA
σ_{cluster} [dB]	3	NA
Small-scale fading		
m_0	0.42[dB]	0.50[dB]
$\widehat{m}_0$	0.31	0.25
$\widetilde{m}_0$	NA	NA
χ	NA	0.86
γ_{rise}	NA	15.21
γ_1	NA	11.84

TABLE III
PARAMETERS FOR CHANNEL MODELS CM 5, CM 6, AND CM 9 (OUTDOOR LOS, OUTDOOR NLOS, AND FARM ENVIRONMENTS)

Outdoor	LOS	NLOS	Farm
valid range of d	$5-17$ m	$5-17$ m	
Path gain			
n	1.76	2.5	1.58
σ_S	0.83	2	3.96
G_0	-45.6	-73.0	-48.96
κ	0.12	0.13	0
Power delay profile			
$\overline{L}$	13.6	10.5	3.31
Λ [1/ns]	0.0048	0.0243	0.0305
λ_1 [1/ns]	0.27	0.15	0.0225
λ_2 [1/ns]	2.41	1.13	NA
β	0.0078	0.062	1
Γ [ns]	31.7	104.7	56
k_γ	0	0	0
γ_0 [ns]	3.7	9.3	0.92
σ_{cluster} [dB]	3	3	3
Small-scale fading			
m_0 [dB]	0.77	0.56	4.1
$\widehat{m}_0$ [dB]	0.78	0.25	2.5
$\widetilde{m}_0$	NA	NA	0

The model for *residential environments* (CM1 and CM 2) was extracted based on measurements that cover a range from 7–20 m, up to 10 GHz. The measurements were done with a vector network analyzer using 1601 frequency points, and using wide-band planar dipole antennas. The antennas were also measured and calibrated in an anechoic chamber and the impact of their frequency response eliminated from the total measured frequency response. At each measurement location, measurements were performed on a 5×5 grid, which allowed the separation of the small-scale and large-scale fading statistics. Measurements were collected in two apartments in Korea in both LOS and NLOS situations. A total of 16 measurement points (each with measurements on a 5×5 grid) was used. More details about those measurements can be found in [33] and [34]; the resulting model parameters are given in Table I. We note that the path-loss exponent for the NLOS situation was taken as an average of the measurements of [34] and other values found in the open literature, especially [51].

For *indoor office environments,* the model was based on measurements that cover a range from 3 to 28 m, 2 to 8 GHz. Specifically, the measurements of [35], which formed the basis for the LOS model as well as some of the parameters for the NLOS model, were done in the frequency range 3–6 GHz, with a vector network analyzer with 1601 frequency points. The used antennas were omnidirectional discone antennas; no separate calibration of the antennas was done in this case. At each location, measurements were taken with a spatial grid of nine points. Measurements were made in an office building with cubicles and rooms, where the cubicles were separated by fabric panels, and the rooms by gypsum material. Further measurements in a corridor and a large lobby in a European office building, with TX-RX separations ranging from 8 to 28 m, were used to parameterize the NLOS case [52]. Especially, those measurements showed a PDP according to (18), and its parameters were established from those measurements. The frequency range of those measurements was 2–8 GHz.

For *outdoor environments,* the measurements cover a range from 5 to 17 m, 3 to 6 GHz [36]. The measurement setup was similar to that of the office environment in [35] described above. The TX was located in the office environment, while the RX was moved to different outdoor locations.[7] No measurements for an outdoor peer-to-peer scenario were available, so that our "outdoor" model is parameterized only based on the "outdoor-to-indoor" measurements.

The model for *industrial environments* was extracted based on measurements [31], [32] that cover a frequency range from 3 to 10 GHz, using a vector network analyzer with 1251 frequency points. Omnidirectional monoconical antennas were used, and their frequency dependence as measured in an anechoic chamber was eliminated from the measurement results.

[7]Note that the FCC allows outdoor UWB devices if they are handheld and battery-powered.

TABLE IV
PARAMETERS FOR CHANNEL MODELS CM 8 AND CM 9 (INDUSTRIAL)

Industrial	LOS	NLOS
valid range of d	$2-8$ m	$2-8$ m
Path gain		
n	1.2	2.15
σ_S [dB]	6	6
G_0 [dB]	-56.7	-56.7
κ	-1.103	-1.427
Power delay profile		
$\overline{L}$	4.75	1
Λ [1/ns]	0.0709	NA
λ [1/ns]	NA	NA
Γ	13.47	NA
k_γ	0.926	NA
γ_0	0.651	NA
σ_{cluster} [dB]	4.32	NA
Small-scale fading		
m_0 [dB]	0.36	0.36
$\widehat{m}_0$ [dB]	1.13	1.15
$\widetilde{m}_0$ dB	12.99	
χ	NA	1
γ_{rise}[ns]	NA	17.35
γ_1 [ns]	NA	85.36

Measurements were performed in a small incinerator hall in Sweden. The hall has a floor area of 13.6×9.1 m and a height of 8.2 m, and was packed with metallic equipment, e.g., pumps, pipes, and cannisters; also, the walls and the ceiling consist of metal, in this case corrugated iron. Measurements were made at distances from 2 to 8 m, with LOS, peer-to-peer NLOS and base-station NLOS scenarios covered. A total of ten measurement points were taken, where at each point measurements were made on a 7×7 grid. The path-loss model also relies on values from the literature [53].

For the farm environment, no measurements were available. Rather, the model is based on the ray-tracing simulations of [54]. Only LOS scenarios were considered, and the frequency dependence of the different reflection and diffraction processes was not explicitly taken into account (for this reason, $\kappa = 0$ in the extracted parameters).

B. Parameterization for <1 GHz

As outlined in the introduction, another important frequency range lies below 1 GHz. Unfortunately, there are few measurements available for this frequency range [55], which is evaluated in [29]; see also [56]. For this reason, only a single type of environment, namely indoor office, could be parameterized. Measurements were made with a pulse generator as TX and a sampling oscilloscope as RX. Antenna effects were calibrated out by recording the signal with a reference antenna that was placed within 1 m from the transmitter with LOS connection. A total of 14 points were measured, where at each point measurements were made on a 7×7 grid.

The environment is described as a dense model, with a single cluster, i.e., $L = 1$, so that $\tau_{k,1} = \tau_k = k \cdot \Delta\tau$, where $\Delta\tau$ is the spacing of the delay taps. The only deviation from the model of Section II is that the first delay bin carries a higher power, so that

$$E\left\{|a_k|^2\right\} = \begin{cases} \frac{G}{1+rF(\varepsilon)} & \text{for } k = 1 \\ \frac{G}{1+rF(\varepsilon)} r e^{-\frac{(\tau_k - \tau_2)}{\varepsilon}} & \text{for } k = 2, \ldots, L_r \end{cases} \tag{24}$$

where

$$F(\varepsilon) = \frac{1}{1 - \exp(-L_r \Delta\tau/\varepsilon)}. \tag{25}$$

This model also includes a dependence of the decay time constant on the distance

$$\varepsilon = (d/10\text{ m})^{0.5} \cdot 40\text{ ns}. \tag{26}$$

This equation gives the same delay spread as the model of [29] at 10 m distance. The distance exponent was chosen as a compromise between the results of Cassioli *et al.* (no distance dependence) and the results of [57] that showed a linear increase with distance.

The power ratio $r_{\text{dB}} = 10\log_{10}(E\{|a_2|^2\}/E\{|a_1|^2\})$ indicates the amount of extra power (compared to the pure exponential decay law) carried in the first bin. It is also modeled as a normal variable with a distribution

$$r_{\text{dB}} \sim \mathcal{N}(-4.0, 3.0) \tag{27}$$

where $\mathcal{N}(x, y)$ is a normal distribution with mean x and standard deviation y.

The small-scale fading is given again by a Nakagami distribution, whose m-factor was chosen identical to the results in [29], even though the bandwidth for which we consider the system is slightly larger than in the original model. However, there were no measurements available on which an estimate for a larger bandwidth could be based.

C. Discussion and Possible Improvements

Even though the model has been accepted for standardization purposes, this of course does not imply that it is the last word in UWB channel modeling. Rather, it is very important to be aware of the limitations of the current model. In the following, we point out several issues that might limit its applicability for specific purposes.

- *Number of measurements:* The number of measurements available for each environment is very small; in most cases, only a single campaign with some 10–20 measurement

points is available. This means that the chosen measurement campaign has an undue influence on the total result. A large number of measurements in different buildings should be used to parameterize each environment more reliably. However, we are not aware of any additional measurements at this point in time. Many of the other restrictions of the model mentioned below are related to the lack of a sufficient number of measurement points.

- *Frequency range:* Some of the measurements do not cover the full frequency range of 3.1–10.6 GHz. Furthermore, no measurements are available that cover this frequency range as well as the <1 GHz range in the same location. This makes it difficult to compare the relative merits of systems in those frequency ranges.
- *Distance dependence of the model parameters:* The model does not describe the distance dependence of the parameters (with the exception of the decay time constant for the <1 GHz range model). This is due to two factors: i) an insufficient number of measurement points to parameterize such a dependence and ii) an increased effort for performing simulations of the system at different distances—a problem that is especially relevant for standardization. As we will see below, the model provides 100 realizations of the channel impulse responses for the purposes of reproducible simulations; if a distance dependence of the parameters would exist, then 100 responses would have to be specified for each distance of interest.
- *Calibration of the antennas:* In most of the measurements, the frequency dependence of the antennas was eliminated by dividing the measured transfer function by the transfer function of the calibration measurement; for the simulations, we simply multiply the transfer functions of the used antenna with the transfer function of the channel. However, this approach neglects that the frequency dependence of channel and antenna can be different in different directions: The exact way of modeling the channel and antennas separately would be to define a frequency-dependent version of the double-directional channel description [58], which defines the directions-of-departure and directions-of-arrival, as well as delays and amplitudes of all MPCs, and to combine it with the frequency-dependent antenna patterns of the transmit and receive antenna patterns.

  The antenna calibration is especially tricky if the antenna pattern changes with frequency. In the industrial measurements, the "enhancement" of higher frequencies (i.e., $\kappa < 0$) is observed when we compare the calibration measurements in the azimuthal plane with measurements in the actual industrial environments. This effect can partly be ascribed to the received power not necessarily being limited to the azimuth plane in the industrial environment, combined with the fact that the antenna gain at high frequencies in the azimuthal plane is low (so that the calibration measurements show a strong decay with frequency), while other elevation angles show a higher antenna gain (so that MPCs with higher elevation are less attenuated). A further consideration of this effect would require measurements that can provide information about the elevation of the MPCs.
- *Frequency dependence of the path gain:* Similarly, we model the frequency-dependent path gain as the product of the frequency dependence and the distance dependence. Extensive measurements should be done to investigate whether this simplification is admissible. Also, the dependence of the shadowing variance on the distance and on the frequency has not been investigated.
- *Directional characteristics:* The model does not describe the double-directional characteristics of the propagation. This would be important for allowing a channel description that can be used in conjunction with arbitrary antennas (see above), and even more for the investigation of UWB systems with multiple antennas.[8]
- *Temporal variations:* No description is given of the temporal variations of the channel. Even for fixed placements of the TX and RX, moving scatterers, or objects temporarily shadowing off certain MPCs, can lead to such variations. However, to our knowledge experimental results are insufficient to allow a parameterization.
- *Random variations of path loss exponent:* Reference [61] showed that the path-loss exponent and the shadowing variance of UWB channels can be modeled as a random variable, whose realization changes from building to building. However, our model does not use this approach, because for many environments, there was an insufficient number of measurements to parameterize such a model. As a matter of fact, most of the measurements that form the basis of our model cover only one or two buildings. While the results of [61] could have been applied to residential (and also office) environments, this would have resulted in different path gain models for those specific environments. However, when more measurement points will be available also for outdoor and industrial environments, the random-exponent model will be superior. The parameters for the sub-1 GHz model are summarized in Table V

IV. Body-Area Network

A. Model Description

Section II presented a generic channel model representing typical indoor and outdoor environments for evaluating 802.15.4a systems. However, simulations and measurements of the radio channel around the human body indicate that some modifications are necessary to accurately model a BAN scenario. Due to the extremely close range and the fact that the antennas are worn on the body, the BAN channel model has different path gain, amplitude distribution, clustering, and interarrival time characteristics compared with the other application scenarios within the 802.15.4a context.

Analysis of the electromagnetic field near the body using a finite-difference time-domain (FDTD) simulator indicated that in the 2–6 GHz range, no energy is penetrating through the body. Rather, pulses transmitted from an antenna diffract around the body and can reflect off of arms and shoulders. Thus, distances between the TX and RX in our path gain model are defined as

[8]Note that for the subgigahertz range, [59] and [60] provide some single-directional evaluations of the measurements of [29] and [55] that form the basis of the 802.15.4a model.

TABLE V
PARAMETERS FOR THE BELOW-1-GHZ (OFFICE) MODEL

	NLOS
Pathloss	
n	2.4
σ_S [dB]	5.9
PL_0	
A_{ant}	3dB
κ [dB/octave]	0
Power delay profile	
$\overline{L}$	1
Λ [1/ns]	NA
λ [1/ns]	NA
Γ	NA
k_γ	NA
γ_0	NA
$\sigma_{cluster}$ [dB]	NA
Small-scale fading	
m_0	3.5
k_m	1/73ns
$\widehat{m}_0$	1.84
$\widehat{k}_m$	1/160ns
$\widetilde{m}_0$ dB	
χ	NA
γ_{rise}[ns]	NA
γ_1 [ns]	NA

TABLE VI
PATH-LOSS MODEL FOR BAN

Parameter for BAN	**Value**
γ	107.8 dB/m
d_0	0.1 m
G_0	-35.5 dB

the distance *around* the perimeter of the body, rather than the straight-line distance *through* the body. The amplitude distributions measured near the body are also different: the lognormal distribution turned out to be best; the parameters of the distribution in the different delay bins are given in Table VII. In addition, the uncorrelated scattering assumption is violated for systems where both the TX and RX are placed on the same body. Our simulations and measurements in an anechoic chamber indicate that there are always two clusters of MPCs due to the initial wave diffracting around the body, and a reflection off of the ground.

TABLE VII
PARAMETERS FOR THE LOGNORMAL DISTRIBUTION OF THE STANDARDIZED BAN

mean and std. dev. of lognormal distribution for BAN						
	front	front	side	side	back	back
Bin	$\mu_{dB}/2$	$\sigma_{dB}/2$	$\mu_{dB}/2$	$\sigma_{dB}/2$	$\mu_{dB}/2$	$\sigma_{dB}/2$
1	5.7	4.7	9.6	6.3	9.2	6.3
2	12.1	4.2	12.9	5.7	12.0	6.5
3	17.0	5.2	16.8	5.2	14.6	6.3
4	20.7	5.1	19.6	5.0	15.1	5.7
5	23.2	5.1	19.6	5.0	18.2	5.4
6	25.6	4.5	24.1	4.8	20.9	5.7
7	28.4	4.6	26.7	5.0	22.7	5.5
8	31.4	4.6	28.9	5.0	23.9	5.2
9	34.5	4.8	30.9	5.2	24.0	5.1
10	37.1	4.7	32.4	5.6	24.9	5.4

The IEEE 802.15.4a model does not include indoor environment reflections from walls, etc.[9] Furthermore, the intercluster arrival times are also deterministic and depend on the exact position of the TXs on the body. To simplify this, we have assumed a fixed average intercluster arrival time depending on the specified scenario. The very short transmission distances result in interpath arrival times that are shorter than the delay resolution of the considered systems; thus a "dense" model (uniformly spaced tapped delay line) was used. The extracted channel parameters depended on the position of the RX on the body. To incorporate this effect easily without having to perform a large number of simulations, only three scenarios are defined, corresponding to a RX placed on the "front," "side," and "back" of the body. The distance ranges for those environments are 0.04–0.17 m, 0.17–0.38 m, and 0.38–0.64 m, respectively.

Implementing this model on a computer involves generating N correlated lognormal variables representing the N different bins, and then applying an appropriate path gain based on the distance between the antennas around the body. This can be accomplished by generating N correlated normal variables, adding the path gain, and then converting from a decibel to linear scale as follows:

$$Y_{\mathrm{dB}} = \mathbf{X} \cdot C_{\mathrm{chol}} - \mathbf{M} + G_{\mathrm{dB}} \tag{28}$$

where $\mathbf{X}$ is a vector of N uncorrelated, unit-mean, unit-variance, normal variables and $\mathbf{C}_{\mathrm{chol}}$ is the Cholesky decomposition of the matrix $\mathbf{C}$. To introduce the appropriate variances and cross-correlation coefficients, this vector is multiplied by the upper triangular Cholesky factorization of the desired covariance matrix $\mathbf{C}$ [62]. The means (a vector $\mathbf{M}$) of each different bin and the large-scale path gain (G_{dB}) are then introduced.

[9]These reflections can be important in some cases when the RX is shadowed by the body. Section IV-B suggests an improved model also incorporating these reflections.

The path gain can be calculated according to the following formula:

$$G_{\mathrm{dB}} = -\gamma(d - d_0) + G_{0,\mathrm{dB}} \tag{29}$$

with γ in units of decibels/meter. The parameters of this path gain model extracted from the simulator and measurements are summarized in Table VI. The means and variances of the lognormal distribution describing the amplitude distributions of each bin are given in Table VII; the covariance matrices $\mathbf{C}$ are not reproduced here for space reasons; they can be found in [50]. The arrival time between the first and second cluster is 8.7 ns for the "front" scenario, 8.0 ns for the "side" scenario, and 7.4 ns for the "back" scenario. The inter-ray-arrival time is fixed to 0.25 ns, as the simulation bandwidth for this channel model is only 4 GHz (note that there are two versions of the model: a preliminary version that used a 2 GHz bandwidth and a final version with 4 GHz bandwidth.

B. Possible Improvements

The FDTD simulations on which we based the standardized model include only electromagnetic waves propagating around the body. However, for indoor environments, also MPCs reflecting off of surrounding scatterers are relevant, and have been observed in very recent experiments [63], [64]. Based on this, we mention here an improved model that describes the complete channel. The model reuses the correlated lognormal model of the previous section to generate components diffracting around the body, and then adds additional components from the surrounding environment using a modified SV model.

Several measurements have been taken in an office environment to extract parameters of the SV model. The TX is placed on the front, and the RX is placed on the front, side, or back of the body. Measurements are taken at several locations in a room. At each location, measurements are made at 49 points, arranged in a 7×7 square grid with 5 cm spacing. Large-scale parameters are obtained from the average over each grid, while small-scale parameters are obtained from individual measurements in each grid. Table IX summarizes the major parameters of the resulting model extracted from measurements taken on different sides around the torso. More details can be found in [65].

Some modifications of the classical SV model are made, indicated by the extra parameters in Table IX. The measurements show that a Weibull distribution with shape parameter α and scale parameter β fits the distribution of the cluster arrival times better than the originally proposed Poisson process. We observed a "dense" arrival of MPCs such that each resolvable component contains significant energy. In this case, the concept of ray arrivals loses its meaning and the impulse response is realized using a tapped delay model as in the previous section.

To generate cluster magnitudes, the original exponential decay model is replaced with a dual slope exponential decay model. Γ_1 represents the cluster decay before an empirically derived breakpoint of 40 ns, and Γ_2 is the decay rate after the breakpoint. A lognormally distributed variation around this trend is observed with standard deviation Γ_σ. We approximate the decay rate of rays within clusters using a single exponential decay γ.

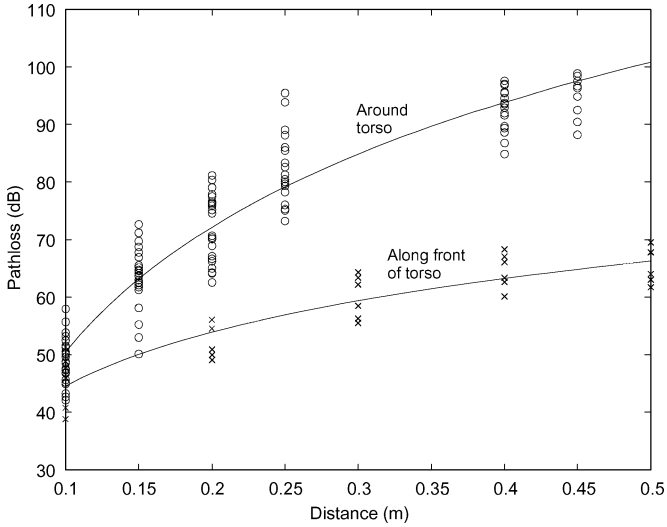

Fig. 1. Path loss in the body-area model.

TABLE VIII
MODEL PARAMETERS FOR DETERMINISTIC CLUSTERS IN BAN

Description	*Parameter*	*Side*	*Back*
Cluster arrival times	T_1, T_2 (ns)	40,80	40,80
Cluster Magnitude	μ_1, μ_2 (dB)	-3.7,-15.0	4.8,-9.2
	σ_1, σ_2 (dB)	4.4,5.8	3.8,6.7

The cluster arrival time and decay parameters in Table IX indicate that the reflected components arrive in several clusters spread out over a long period of time. This is in contrast to the components diffracting near the body, which consist of only two rapidly decaying clusters due to the initial arriving components and the ground reflections.

The large-scale fading of the total reflected energy on the front, back, and side of the body assumes a lognormal distribution with parameters μ_{tot} and σ_{tot}. Comparing the large-scale fading parameters of Table IX with Fig. 1 shows that if the antennas are placed on the same side of the body, the received energy due to components reflected from the indoor environment is significantly smaller than the initial components diffracting near the body. However, if antennas are placed on different sides of the body, the energy of reflected components can dominate the total received power. Fig. 1 also shows that an exponential law (a straight line) for the path gain works best for small distances (including antenna distances <0.1 m not shown in the graph), while for larger distances, a power law might be better. Due to the different propagation mechanisms different pathloss laws are expected depending on whether we consider diffraction around a body part or propagation along a body part [64].

In addition to the random clusters of MPCs, two deterministic clusters are added to take into account reflections off of the front and back walls due to the particular geometry of our

TABLE IX
MODEL PARAMETERS FOR OFFICE CLUSTERS (IMPROVED BAN MODEL)

Description	*Parameter*	*Front*	*Side*	*Back*
Cluster arrival time	α (ns)	2.21	2.11	2.33
	β (ns)	5.0	7.9	5.1
Cluster Decay	Γ_1, Γ_2 (dB/ns)	0.15,0.52	0.19,0.33	0.11,-
	Γ_σ (dB)	3.3	4.1	2.7
Ray Decay	γ (dB/ns)	2.4	1.5	1.3
Large Scale Fading	μ_{tot} (dB)	-69.1	-72.6	-77.5
	σ_{tot} (dB)	0.9	3.1	2.5
Small Scale Fading	μ (dB)	-1.6	-1.6	-1.6
	σ (dB)	4	4	4

office environment (see Table VIII). These clusters are only observed when the RX is on the side or back of the body and do not follow the general trends given in Table IX. The first and second deterministic clusters arrive at an excess delay of $T_1 = 40$ ns and $T_2 = 80$ ns, respectively. Instead of the usual cluster decay law, these cluster magnitudes have lognormal distribution with means $\mu_{1,2}$ and standard deviations $\sigma_{1,2}$.

V. IMPLEMENTATION CONSIDERATIONS

The above specifications are a complete description of the model. In order to help a practical implementation, the following procedure suggests a "cooking recipe" for the implementation of the high frequency model.

- If the model for the specific environment has the SV shape, proceed the following way:
  - — Generate a Poisson-distributed random variable L with mean $\overline{L}$. This is the number of clusters for the considered realization.
  - — Create $L-1$ exponentially distributed variables x_n with decay constant Λ. The times $\sum_{n=1}^{l} x_n$ give the arrival times of the first components of the lth cluster.
  - — For each cluster, generate the cluster decay time and the total cluster power, according to (16) and (17), respectively.
  - — For each cluster, generate the path arrival times:
    - If the path arrival times follow a standard Poisson distribution, generate a number of exponentially distributed (with decay constant $1/\lambda_1$) random numbers y_n, which are the path interarrival times, i.e., the delay between the nth and the $(n+1)$th path.
    - If the path arrival times follow a mixed Poisson processes, obtain y_n as follows: first generate a realization of a random variable from a distribution that is uniform between zero and one. If that variable is smaller than β, then generate y_n from an exponential distribution with decay constant $1/\lambda_1$; otherwise, generate y_n from an exponential distribution with decay constant $1/\lambda_2$.
    - The arrival time of the kth path is $\sum_{n=1}^{k} y_n$. The actual number of considered components depends on the required dynamic range of the model.
  - — For each component, compute the mean power according to (15).
- For the office NLOS or the industrial NLOS, compute the mean power according to (18); note that the components arrive at regularly spaced intervals that are multiples of the inverse system bandwidth.
- For each first component of the cluster, set the m-factor to $\widetilde{m}_0$; for industrial environments, only set the m-factor of the first component of the first cluster to $\widetilde{m}_0$.
- For all other components, compute the mean and the variance of the m-factor according to (21) and (22).
- For each component, compute the realization of the amplitude as a Nakagami-distributed variable with mean-square given by the mean power of the components as computed three steps above, and m-factor as computed one step above.
- Compute the phase for each component as uniformly distributed.
- Filter the signal to the desired system bandwidth (e.g., 500 MHz, 1.5 GHz, etc.)
- Apply a filtering with a $f^{-\kappa}$ filter.
- Resample the signal with the desired simulation sampling frequency.
- Make sure that the above description results in a profile that has *average* power of one1, i.e., has unit power when averaged over all the different random processes.
- For the simulation of the actual system, multiply the (frequency-dependent) transfer function of the channel with the frequency-dependent path gain, the frequency-dependent antenna characteristics, and the emission spectrum.

In order to simplify simulations, and to guarantee reproducible and comparable results, 100 impulse responses have been created for each of the nine environments of the high-frequency channel models. Those models are given, in a time-discrete form, in Excel tables that can be found at www.802wirelessworld.com. This site also contains a MATLAB program with an implementation of the model; the program is also contained in [50].

For the low-frequency model, we have the added difficulty that the shape of the impulse response changes with distance. In order to generate impulse responses at various distances, the following procedure should be used: the stored impulse responses have all the same average power in the different delay taps (with the exception of the first component, which is chosen according to the ratio r). For the simulation, we then compute the decay time constant for a chosen distance d according to $\varepsilon = (d/10\text{ m})^{0.5} \cdot 40$ ns and attenuate the samples of the stored impulse responses with $\exp(-\tau/\varepsilon)$. Subsequently, the newly created impulse responses are normalized to unit total energy. For the BAN model, implementation considerations are discussed in [66].

VI. SIMULATION RESULTS

The parameterized channel models can be used to generate ensembles of impulse responses, which in turn are employed to test the performance of different UWB transceiver structures. In the following, we present some example realizations, as well as parameters that allow insight into the effects of the impulse

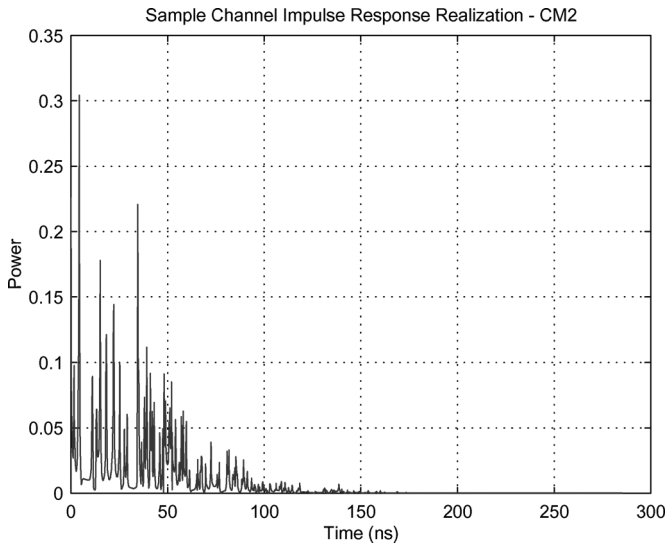

Fig. 2. Impulse response realization in CM2 (residential NLOS).

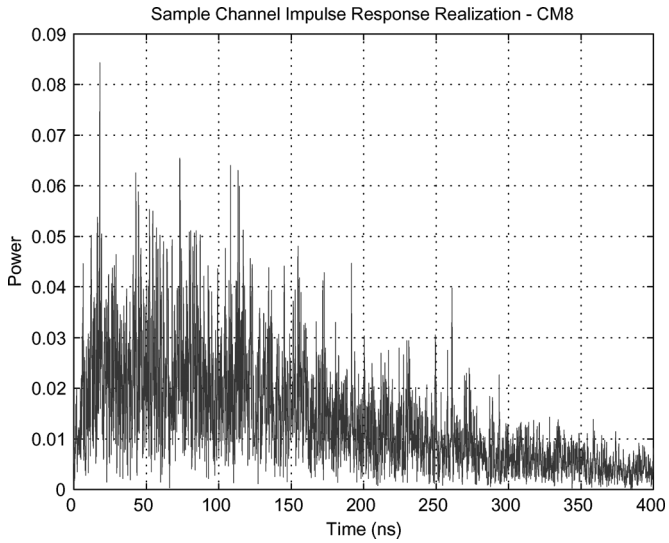

Fig. 3. Impulse response realization in CM8 (industrial NLOS).

response on Rake RXs, which are used for combining different MPCs in both impulse-radio based systems and direct-sequence spread-spectrum systems. Those example results are all drawn from the high-frequency models.

The impulse responses in different environments have some noticeable differences between them. Fig. 2 depicts a typical instantaneous PDP $|h(\tau)|^2$ in a residential NLOS situation (CM2). We see clearly the separation between the MPCs and the arrival in clusters. This arises from the use of the SV model (with modified MPC arrival statistics) as described in Section II. A strong contrast to this is the impulse responses in the industrial NLOS environment in Fig. 3. In this example, we first observe that the first arriving MPC is strongly attenuated, and the maximum in the instantaneous PDP occurs only after about 50 ns. This is especially significant for ranging and geolocation applications, since the ranging requires the detection of the *first* path, not of the strongest path. Detection of such a weak component in a noisy environment can be quite challenging.

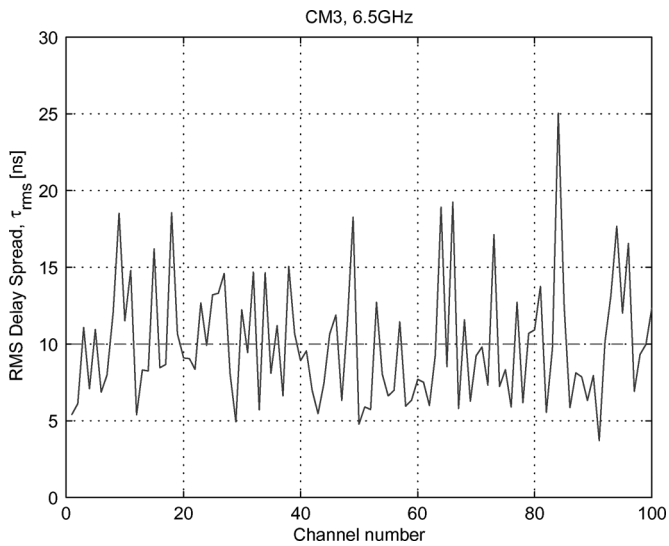

Fig. 4. RMS delay spread of the different channel realizations in CM 3.

It is interesting to note that while the energy contained within each impulse response does not change, the root mean square delay spread can show significant variations, as shown in Fig. 4 for office LOS (CM3). The reason for this is that MPCs at different delays are especially strong for the different realizations, thus giving different values of the delay spread.

From the impulse responses, we can also derive some auxiliary parameters that have great importance for the design of Rake RXs. These parameters are the number of MPCs within 10 (or 20) dB within the amplitude of the strongest received signal and the number of MPCs that contain 50% (or 90%) of the received energy. Especially the latter gives guidelines for the number of Rake fingers that have to be used to obtain an appreciable SNR ratio. Table X summarizes the mean values of those parameters for a filter bandwidth of 6.5 GHz. Similar results for the BAN model are shown in Table XI. Also, the variations of those numbers of MPCs can be considerable from channel realization to channel realization. Fig. 5 shows the cumulative distribution function of the number of significant paths for the residential LOS (CM1) and outdoor NLOS (CM6) environments.

The above figures are only a small sample of the results that can be obtained with this channel model. Extensive simulations of some 20 different systems have been performed as part of the IEEE 802.15.4a standardization activities.

VII. Summary and Conclusions

We have presented a comprehensive model for UWB propagation channels that was accepted as standardized model by IEEE 802.15.4a. The model is based on a large number of measurement and simulation campaigns and includes the most important propagation effects in UWB channels, including the frequency selectivity of the path loss, stochastic interarrival times of the MPCs, and a soft onset of the PDP in some NLOS situations. The model allows to test a wide variety of UWB transceivers in a unified and reproducible way.

We have also discussed the limits of applicability and possibilities for future improvement and generalization. However, at

TABLE X
EFFECTIVE PARAMETERS FOR A SYSTEM BANDWIDTH OF 6.5 GHz

CM	Mean τ_{rms}	Mean NP10dB	Mean NP20dB	Mean NP50%	Mean NP90%
1	17	15.6	80.5	9.5	79.0
2	19	35.1	176.4	22.5	154.6
3	10	22.7	85.1	10.4	57.7
4	13	53.1	228.6	30.5	160.4
5	29	24.4	116.7	13.8	98.0
6	75	33.4	170.0	21.5	159.7
7	8	11.3	48.8	5.5	40.2
8	89	320.5	1442.1	251.4	1066.6
9	21	4.6	15.2	2.0	8.3

TABLE XI
EFFECTIVE PARAMETERS OF A BODY-AREA SYSTEM WITH A BANDWIDTH OF 4 GHz. METRICS ARE PROVIDED FOR THE DIFFRACTING COMPONENTS ONLY (WHICH IS THE MODEL UNDERLYING THE STANDARD)/ AND THE CHANNEL CONSISTING OF DIFFRACTING AND GROUND-REFLECTED COMPONENTS

CM	Mean τ_{rms}	Mean NP10dB	Mean NP20dB	Mean NP50%	Mean NP90%
1	0.2 / 0.6	2.4 / 2.5	4.3 / 4.5	1.1 / 1.1	2.5 / 2.6
2	0.3 / 1.1	3.1 / 3.4	6.7 / 7.5	1.4 / 1.5	3.6 / 3.8
3	0.5 / 1.6	5.4 / 5.1	10.8 / 11.3	2.1 / 1.9	5.8 / 5.9

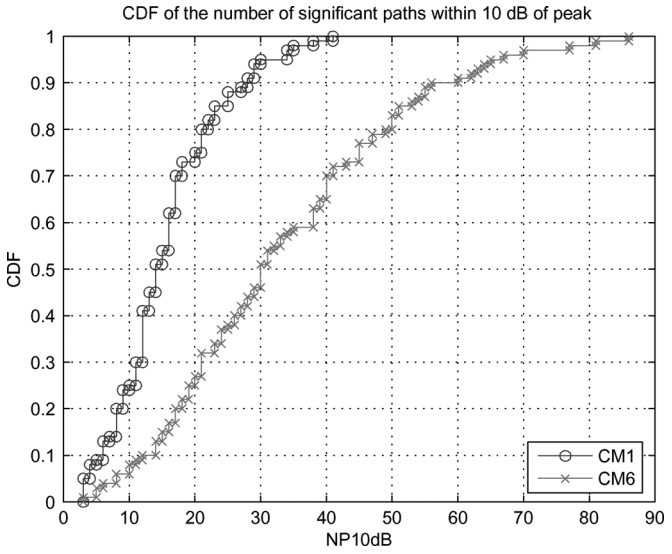

Fig. 5. Cumulative distribution function of the number of paths within 10 dB of the strongest path in CM1 (residential LOS) and CM6 (outdoor NLOS).

this point in time, the model is the most comprehensive UWB channel model available and has been used successfully in establishing a UWB standard for sensor network communications.

ACKNOWLEDGMENT

Stimulating discussions with the IEEE 802.15.4a Task Group, and the support of its Chairman P. Kinney and Vice Chair J. Ellis are gratefully acknowledged. The discussions with, and suggestions by, U. Schuster have greatly enriched this paper.

REFERENCES

[1] L. Fullerton, "Time domain transmission system," U.S. Patent 4 813 057, 1989, Tech. Rep.

[2] R. A. Scholtz, "Multiple access with time-hopping impulse modulation," in *Proc. IEEE Military Commun. Conf. (MILCOM)*, Boston, MA, Oct 1993, vol. 2, pp. 447–450.

[3] M. Z. Win and R. A. Scholtz, "Impulse radio: How it works," *IEEE Commun. Lett.*, vol. 2, pp. 36–38, Feb 1998.

[4] ——, "Ultra-wide bandwidth time-hopping spread-spectrum impulse radio for wireless multiple-access communications," *IEEE Trans. Commun.*, vol. 48, pp. 679–691, Apr 2000.

[5] M. Z. Win, "A unified spectral analysis of generalized time-hopping spread-spectrum signals in the presence of timing jitter," *IEEE J. Sel. Areas Commun.*, vol. 20, pp. 1664–1676, Dec 2002.

[6] A. Ridolfi and M. Z. Win, "Ultrawide bandwidth signals as shot-noise: A unifying approach," *IEEE J. Sel. Areas Commun.*, vol. 24, pp. 899–905, Apr 2006.

[7] M. G. diBenedetto, T. Kaiser, A. F. Molisch, I. Oppermann, C. Politano, and D. Porcino, Eds., *UWB Communications Systems: A Comprehensive Overview*. Hindawi: EURASIP, 2005.

[8] R. C. Qiu, H. Liu, and X. Shen, "Ultra-wideband for multiple access communications," *IEEE Commun. Mag.*, vol. 43, pp. 80–87, Feb. 2005.

[9] L. Yang and G. B. Giannakis, "Ultra-wideband communications—An idea whose time has come," *IEEE Signal Process. Mag.*, vol. 21, pp. 26–54, Nov. 2004.

[10] A. Giorgetti, M. Chiani, and M. Z. Win, "The effect of narrowband interference on wideband wireless communication systems," *IEEE Trans. Commun.*, vol. 53, pp. 2139–2149, Dec 2005.

[11] M. Z. Win, G. Chrisikos, and N. R. Sollenberger, "Performance of Rake reception in dense multipath channels: Implications of spreading bandwidth and selection diversity order," *IEEE J. Sel. Areas Commun.*, vol. 18, pp. 1516–1525, Aug 2000.

[12] T. Q. S. Quek and M. Z. Win, "Analysis of UWB transmitted reference communication systems in dense multipath channels," *IEEE J. Sel. Areas Commun.*, vol. 23, pp. 1863–1874, Sep 2005.

[13] W. Suwansantisuk, M. Z. Win, and L. A. Shep, "On the performance of wide-bandwidth signal acquisition in dense multipath channels," *IEEE Trans. Veh. Technol.*, vol. 54, pp. 1584–1594, Sep 2005.

[14] A. Batra *et al.*, Multi-band OFDM Physical Layer Proposal 2003, Doc. IEEE 802.15-03/267r2.

[15] J. McCorkle *et al.*, Xtreme Spectrum cpf Document 2003, Doc. IEEE 802.15-03/154r0.

[16] M. Z. Win and R. A. Scholtz, "On the energy capture of ultra-wide bandwidth signals in dense multipath environments," *IEEE Commun. Lett.*, vol. 2, pp. 245–247, Sept 1998.

[17] ——, "On the robustness of ultra-wide bandwidth signals in dense multipath environments," *IEEE Commun. Lett.*, vol. 2, pp. 51–53, Feb 1998.
[18] ——, "Characterization of ultra-wide bandwidth wireless indoor communications channel: A communication theoretic view," *IEEE J. Sel. Areas Commun.*, vol. 20, pp. 1613–1627, Dec 2002.
[19] S. Gezici, Z. Tian, G. B. Giannakis, Z. Sahinoglu, H. Kobayashi, A. F. Molisch, and H. V. Poor, "Ultra-wideband positioning," *IEEE Trans. Signal Process.*, vol. 22, no. 4, pp. 70–84, 2005.
[20] I. Guvenc, H. Arslan, S. Gezici, and H. Kobayashi, "Adaptation of multiple access parameters in time hopping uwb cluster based wireless sensor networks," in *Proc. Int. Conf. Mobile Ad-hoc Sensor Syst.*, Oct. 2004, pp. 235–244.
[21] A. F. Molisch, *Wireless Communications*. New York: IEEE Press/ Wiley, 2005.
[22] R. C. Qiu, "Propagation effects," in *UWB Communications Systems: A Comprehensive Overview*, M. G. Di Benedetto, Ed. Lausanne, Switzerland: EURASIP, 2005.
[23] A. H. Muqaibel, "Characterization of ultra wideband communication channels," Ph. D. thesis, Virginia Polytechnic Univ., Blacksburg, VA, Mar. 2003.
[24] A. F. Molisch, "Ultrawideband propagation channels—Theory, measurement, and modeling," *IEEE Trans. Veh. Technol.*, vol. 54, pp. 1528–1545, Sep. 2005.
[25] A. F. Molisch and F. Tufvesson, "Multipath propagation models for broadband wireless systems," in *CRC Handbook of Signal Processing for Wireless Commmunications*, M. Ibnkahla, Ed. Boca Raton, FL: CRC Press, 2004.
[26] D. R. McKinstry, "Ultra-wideband small scale channel modeling and its application to receiver design," M.Sc. thesis, Virginia Polytechnic Univ., Blacksburg, Jun. 2003.
[27] W. Q. Malik, "An holistic approach to optimal ultra-wideband wireless communications system design," Ph.D. dissertation, Oxford Univ., Oxford, U.K., 2005.
[28] R. C. Qiu, "A generalized time domain multipath channel and its application in ultra-wideband (UWB) wireless optimal receiver design: wave-based system ananlysis," *IEEE Trans. Wireless Commun.*, vol. 4, pp. 2312–2324, 2004.
[29] D. Cassioli, M. Z. Win, and A. F. Molisch, "The ultra-wide bandwidth indoor channel—From statistical model to simulations," *IEEE J. Sel. Areas Commun.*, vol. 20, pp. 1247–1257, Aug 2002.
[30] A. F. Molisch, J. R. Foerster, and M. Pendergrass, "Channel models for ultrawideband personal area networks," *IEEE Wireless Commun.*, vol. 10, pp. 14–21, Dec. 2003.
[31] J. Karedal, S. Wyne, P. Almers, F. Tufvesson, and A. F. Molisch, "Channel measurements and modeling of an ultra-wideband industrial channel," *IEEE Trans. Wireless Commun.*, 2006.
[32] ——, "Statistical analysis of the UWB channel in an industrial environment," in *Proc. IEEE Veh. Tech. Conf. (VTC-Fall)*, Los Angeles, CA, Sept. 2004, vol. 1, pp. 81–85.
[33] C.-C. Chong and S. K. Yong, "A generic statistical-based UWB channel model for high-rise apartments," *IEEE Trans. Antennas Propag.*, vol. 53, pp. 2389–2399, Aug 2005.
[34] C.-C. Chong, Y.-E. Kim, S. K. Yong, and S.-S. Lee, "Statistical characterization of the UWB propagation channel in indoor residential environment," *Wireless Commun. Mobile Comput.*, vol. 5, pp. 503–512.
[35] B. Kannan *et al.*, UWB channel characterization in office environments Tech. Rep. Doc. IEEE 802.15-04-0439-00-004a, 2004.
[36] ——, UWB channel characterization in outdoor environments Tech. Rep. Doc. IEEE 802.15-04-0440-00-004a, 2004.
[37] Federal Communications Commission, First Rep. Order 02-48 2002.
[38] R. Kohno, Interpretation and future modification of japanese regulation for UWB Tech. Rep. Doc. IEEE 802.15-06-0140-01-004a, 2005.
[39] A. F. Molisch *et al.*, Merged UWB proposal for IEEE 802.15.4a Alt-PHY Tech. Rep. IEEE 802.15-05-0158-00-004a, 2005.
[40] B. Denis, J. Keignart, and N. Daniele, "UWB measurements and propagation models for snowy environments," in *Proc. IEEE Intl. Conf. Ultra-Wideband (ICU)*, Zurich, Switzerland, Sept 2005, pp. 118–123.
[41] P. Bello, "Characterization of randomly time-variant linear channels," *IEEE Trans. Commun.*, vol. 11, pp. 360–393, 1963.
[42] R. C. Qiu and I.-T. Lu, "Wideband wireless multipath channel modeling with path frequency dependence," in *Proc. IEEE Int. Conf. Commun.*, Dallas, TX, Jun. 1996, pp. 277–281.
[43] ——, "Multipath resolving with frequency dependence for broadband wireless channel modeling," *IEEE Trans. Veh. Technol.*, vol. 48, pp. 273–285, Jan 1999.
[44] H. Schantz, *The Art and Science of Ultra-Wideband Antennas*. Reading, MA: Artech House, 2005.
[45] J. O. Nielsen, G. F. Pedersen, K. Olesen, and I. Z. Kovacs, "Statistics of measured body loss for mobile phones," *IEEE Trans. Antennas Propag.*, vol. 49, pp. 1351–1353, Sep. 2001.
[46] A. A. M. Saleh and R. A. Valenzuela, "A statistical model for indoor multipath propagation," *IEEE J. Sel. Areas Commun.*, vol. 5, pp. 128–137, Feb. 1987.
[47] L. Correia, *Wireless Flexible Personalized Communications*. New York: Wiley, 2001.
[48] W. C. Jakes, *Microwave Mobile Communications*. New York: IEEE Press, 1974.
[49] G. L. Stueber, *Principle of Mobile Communication*. Norwell, MA: Kluwer, 1996.
[50] A. F. Molisch *et al.*, IEEE 802.15.4a channel Model—Final report Tech. Rep. Doc. IEEE 802.15-04-0662-02-004a, 2005.
[51] U.C.A.N., Radio channel sounding results and model Tech. Rep. IST-2001-32710, Nov. 2002, deliverable D31.
[52] U. Schuster, Channel Measurements In Office Environments Doc. IEEE 802.15-04-0447-00-004a, 2004.
[53] T. S. Rappaport, S. Y. Seidel, and K. Takamizawa, "Statistical channel impulse response models for factory and open plan building radio communication system design," *IEEE Trans. Commun.*, vol. 39, pp. 794–807, May 1991.
[54] S. Emami *et al.*, Channel parameters for farm/open-area applications Tech. Rep. Doc. IEEE 802.15-04-0475-00-004a, 2005.
[55] M. Z. Win, "Ultra-wide bandwidth spread-spectrum techniques for wireless multiple-access communications," Ph.D. dissertation, Univ. of Southern California, , May 1998.
[56] D. Cassioli, "Ultra-wideband wireless communication systems: from the statistical propagation model to simulations and performance analysis," Ph.D. dissertation, Univ. of Rome Tor Vergata, Italy, 2003.
[57] K. Siwiak, H. Bertoni, and S. M. Yano, "Relation between multipath and wave propagation attenuation," *Electron. Lett.*, vol. 39, pp. 142–143, Jan. 2003.
[58] M. Steinbauer, A. F. Molisch, and E. Bonek, "The double-directional radio channel," *IEEE Antennas Propag. Mag.*, vol. 43, pp. 51–63, Aug 2001.
[59] R. J.-M. Cramer, "An evaluation of ultra-wideband propagation channels," Ph.D. dissertation, Univ. of Southern California, , Dec. 2000.
[60] R. J.-M. Cramer, R. A. Scholtz, and M. Z. Win, *Eval. Ultra-Wide-Band Propag. Channel*, vol. 50, pp. 561–570, May 2002.
[61] S. Ghassemzadeh, R. Jana, C. Rice, W. Turin, and V. Tarokh, "Measurement and modeling of an ultra-wide bandwidth indoor channel," *IEEE Trans. Commun.*, vol. 52, pp. 1786–1796, Oct 2004.
[62] G. H. Golub and C. F. V. Loan, *Matrix Computations*. Baltimore, MD: John Hopkins Univ. Press, 1989.
[63] T. Zasowski, F. Althaus, M. Stager, A. Wittneben, and G. Tröster, "UWB for noninvasive wireless body area networks: Channel measurements and results," in *IEEE Conf. Ultra-Wideband Syst. Technol. (UWBST)*, Reston, VA, Nov. 2003, pp. 285–289.
[64] A. Fort, C. Desset, J. Ryckaert, P. DeDoncker, L. VanBiesen, and P. Wambacq, "Characterization of the ultra wideband body area propagation channel," in *Proc. IEEE Int. Conf. Ultra-Wideband (ICU)*, Zurich, Switzerland, Sep. 2005, pp. 22–27.
[65] A. Fort, J. Ryckaert, C. Desset, P. D. Doncker, and L. V. Biesen, "Ultra wideband channel model for communication around the human body," *IEEE J. Sel. Areas Commun.*, vol. 24, pp. 927–933, Apr. 2006.
[66] A. Fort, C. Desset, P. Wambacq, and L. Van Biesen, "Body area RAKE receiver communication," in *IEEE Conf. Commun. (ICC)*, Istanbul, Turkey, Jun. 2006.

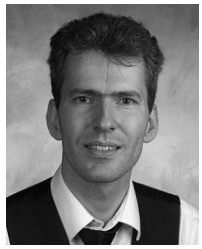

Andreas F. Molisch (S'89–M'95–SM'00–F'05) is a Distinguished Member of Technical Staff with Mitsubishi Electric Research Labs, Cambridge, MA. He is also Professor and Chairholder for radio systems at Lund University, Sweden. Previously, he was with the Technical University of Vienna, FTW, and AT&T (Bell) Labs—Research. His current research interests are measurement and modeling of mobile radio channels, UWB, cooperative communications, and MIMO systems. He has authored, coauthored, or edited four books, among them *Wireless Communications* (New York: Wiley-IEEE Press), 11 book chapters, some 95 journal papers, and numerous conference contributions.

Prof. Molisch has been Chairman of various international organizations, Editor and Guest Editor for IEEE TRANSACTIONS ON WIRELESS COMMUNICATIONS and IEEE JOURNAL ON SELECTED TOPICS IN COMMUNICATIONS, and Chair of several conferences and symposia. He has received a number of awards.

Dajana Cassioli (S'02–M'04) received the "Laurea" and Ph.D. degrees from the University of Rome Tor Vergata, Italy, in 1999 and 2003, respectively.

From 1998 to 1999, she was with the Fondazione Ugo Bordoni, Rome, Italy. In 1999, she joined the Communication Group of the Electronic Engineering Department at the University of Rome Tor Vergata, where she has been working on the analysis and simulation of the UMTS. She is currently with RadioLabs, a university-industry research consortium for the development of radio technologies, where she is the director of the associate laboratory at the University of L Aquila, Italy. Her main research interests are in the field of wireless access technologies, and in particular UWB technology and ad-hoc networks. In the year 2000, she was a Summer Manager with the Wireless Systems Research Department at AT&T Labs-Research, working on the statistical analysis of UWB signal propagation

Chia-Chin Chong (S'00–M'03) received the Ph.D. degree in electrical engineering from the University of Edinburgh, U.K., in 2003.

From 2004 to 2005, she was with Samsung Advanced Institute of Technology, Korea. Since then, she has been with DoCoMo Communications Laboratories USA, Palo Alto, CA. She has done research in the areas of channel parameter estimations, propagation channel measurements and modeling, and UWB systems. She has published numerous international journals, conference papers, and IEEE standard contributions. She is an Editor for *Wireless Personal Communications* and the *EURASIP Journal on Wireless Communications and Networking* (JWCN), for which she was a Guest Editor for the Special Issue on Millimeter Wave.

Dr. Chong has served on the Technical Program Committee (TPC) of various international conferences and was TPC Co-Chair for the Wireless Communications Symposium of IEEE ICC 2008.

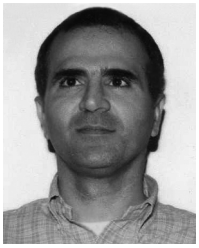

Shariar Emami (M'91–SM'00) received the B.S.E.E., M.S., and Ph.D. degrees from the University of Florida, Gainesville, all in electrical Engineering, in 1986, 1987 and 1993, respectively.

From January to August 1994, he was a visiting Assistant Professor with the Department of Electrical Engineering, University of North Florida. He was with Motorola Inc. from 1994 to 2004 where he worked on various radio communication technologies. He then joined Freescale in 2004 where he was involved in research and development on ultrawideband and WPAN solutions. He is currently a Senior Member of technical staff at Focus Enhancements Semiconductor, Hillsboro, OR. He holds seven issued patents

Dr. Emami is a member of Eta Kappa Nu. He has served on technical program committees of several international conferences and.

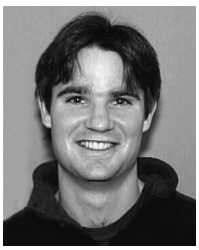

Andrew Fort (M'04) was born in Ottawa, ON, Canada in 1975. He received the bachelor's degree in computer and electrical engineering from the University of Victoria, BC, Canada in 1998.

He was with IVL Technologies, Victoria, designing DSP algorithms for pitch recognition of the human voice. He joined IMEC, Belgium, in January 2000 and was involved in the research and development of a wide range of communication systems, including satellite and wireless local-area networks. Since January 2004, he is conducting doctoral studies at the Vrije Universiteit Brussel on ultra-low-power medical sensors under the supervision of Prof. L. Van Biesen.

Balakrishnan Kannan (M'02) was born in Sri Lanka. He received the B.Sc. and B.Eng. degrees from the University of Sydney, Australia, in 1994 and 1995, respectively, and the Ph.D. degree in electrical engineering from Cambridge University, U.K., in 2001.

He was with Motorola, Singapore, as an Electronic Engineer for two years and the Institute for Infocomm Research, A*Star, Singapore, as a Scientist for five years. Currently, he is a Research Fellow at the University of New South Wales, Australia. His research interests include array signal processing, space-time coding, MIMO systems, and UWB impulse radio. He has published around 45 papers in international conferences and journals.

Dr. Kannan was Secretary of the IEEE Singapore Section Communications Chapter in 2002 and 2003 and Treasurer for the 7th IEEE International Conference on Communication Systems (ICCS'02).

Johan Karedal (S'01) received the M.S. degree in engineering physics from Lund University, Sweden, in 2002, where he is currently pursuing the Ph.D. degree in the Department of Electroscience.

His research interests are in channel measurement and modeling for MIMO and UWB systems.

Jurgen Kunisch photograph and biography not available at the time of publication.

Hans Gregory Schantz (M'95–SM'04) was born in Detroit, MI, on September 27, 1966. He received degrees in engineering and physics from Purdue University, West Lafayette, IN, in 1988 and 1990, respectively. He received the Ph.D. degree in theoretical physics from the University of Texas at Austin in 1995.

His work experience includes stints with IBM, the Lawrence Livermore National Laboratory, and the ElectroScience Lab of The Ohio State University. In 1999, he joined the Time Domain Corp., Huntsville, AL, as an Antenna Engineer. His pioneering work in UWB antennas led to more than a dozen patents. He is the author of *The Art and Science of Ultrawideband Antennas* (Norwood, MA: Artech House, 2005). Since 2002 he has been a Consulting Engineer for Next-RF, Inc. as well as Chairman and Chief Technology Officer for the Q-Track Corporation, both in Huntsville. His research interests include electromagnetic energy flow, UWB antennas, electrically small antennas, and low-frequency near-field systems and propagation.

Dr. Schantz organized the Huntsville Joint Chapter of the IEEE Communications, Antennas and Propagation, and Microwave Theory and Techniques Societies in 2002. He is the current Chair of this Joint Chapter.

Kazimierz (Kai) Siwiak (SM'84) is Founder and CEO of TimeDerivative, Inc., a wireless technology venture. He was previously Vice President of Strategic Development with Time Domain Corp. He consults on wireless systems, antennas, propagation, IEEE802 and other standards, ITU-R representation, UWB development, and lectures globally about UWB technology and antennas and propagation. He holds more than 70 patents, with 31 issued in the United States, and has published extensively, including (with D. McKeown) *Ultra-Wideband Radio Technology* (New York: Wiley, 2004) and *Radiowave Propagation and Antennas for Personal Communications* (Reading, MA: Artech, 1995). He is an avid amateur Radio Operator and a commercial Airplane Pilot with instrument and multiengine ratings.

Dr. Siwiak recently received the Dan Noble Fellow and the Silver Quill Awards from Motorola Corporation, where he was named Master Innovator.

Moe Z. Win (F'04) is an Associate Professor at the Massachusetts Institute of Technology (MIT), Cambridge. Prior to joining MIT, he spent five years with AT&T Research Laboratories and seven years with the Jet Propulsion Laboratory, Pasadena, CA.

Prof. Win is an IEEE Distinguished Lecturer. He is the current Chair and past Secretary (2002–2004) for the Radio Communications Committee of the IEEE Communications Society. He is Area Editor for Modulation and Signal Design and Editor for Wideband Wireless and Diversity for the IEEE TRANSACTIONS ON COMMUNICATIONS. He has received several awards, including the Presidential Early Career Award for Scientists and Engineers from the White House and the IEEE Eric E. Sumner Award "for pioneering contributions to ultrawideband communications science and technology."